# An investigation of spectral collocation boundary element method for the computation of exact Green's functions in acoustic analogy

Andrea D. Jones, Fang Q. Hu<sup>†</sup>

\*†Old Dominion University, Norfolk, Virginia 23529, USA

A spectral collocation boundary element method (BEM) is used to solve for the exact Green's function and its double divergence numerically. Exponential rate of convergence is demonstrated for smooth boundaries. The advantage of using high-order orthogonal polynomials as basis functions is shown through a Nodes per Wavelength calculation. For field points close to the boundary, the double divergence is computed both by direct differentiation and by using finite difference stencils. The preferred method for calculating the double divergence at all field points is found to be direct computation. Results of using the spectral collocation BEM on a square boundary without proper treatment of corner singularities are shown with non-exponential rates of convergence. Geometric discontinuities are dealt with by means of an exponentially graded mesh refinement on corner elements. Several refinement strategies are compared. Exponential rate of convergence is demonstrated for a square boundary using a refinement ratio of 0.35. Finally, an example is presented comparing the predicted sound field obtained by using the exact Green's function with that of a direct time-domain finite difference solution.

### I. Introduction

A Green's function that satisfies all the boundary conditions is often referred to as the exact or the tailored Green's function. It is well known in the theory of acoustic analogy that when an exact Green's function is used, the far field sound can be expressed as a volume integral involving the Lighthill tensors and the double divergence of the Green's function. Although it is not necessarily more efficient computationally to use the volume integral compared to the surface integral in the Ffowcs Williams-Hawkings equation in which the free space Green's function is employed, the use of the exact Green's function allows the development of noise prediction strategy based on steady flow simulations with direct noise source modelings.<sup>3</sup> The computation of the exact Green's function, as well as its double divergence, becomes an integral part of this noise prediction strategy.

Recently, a high-order boundary element method for the exact Green's function using Chebychev polynomials has been proposed in [5]. Although the Boundary Element Method has been applied to the Helmholtz equation for several decades, most existing numerical methods were limited to the use of constant or linear elements. The use of high-order basis polynomials has several advantages. In addition to a significant increase in computational efficiency and accuracy, the use of high-order basis functions can accurately approximate the tangential derivative of the unknown function in the presence of the mean flow; Since the collocation points are chosen to be interior Gauss points, evaluation of the boundary integral equation on the corner

<sup>\*</sup>Graduate student, Department of Mathematics and Statistics, student member AIAA

<sup>&</sup>lt;sup>†</sup>Professor, Department of Mathematics and Statistics, Senior member AIAA

Copyright ©2006 by the American Institute of Aeronautics and Astronautics. All rights reserved.

points are avoided; The accuracy of the solution can be quickly assessed by the magnitudes of the expansion coefficients; The use of high-order basis functions does not increase computational complexity when compared with constant or linear elements, because the final linear algebraic systems always have dense matrices in all methods.

In the present paper, we further improve the spectral collocation method proposed in [5]. In particular, with a proper treatment of solution singularities at geometric discontinuities, exponential rate of convergence will be demonstrated by the use of a graded element refinement near the corner points.<sup>6, 10</sup> Different refinement strategies are studied and compared. Moreover, effective computation of the double divergence of the Green's function will be studied and the best strategy for its numerical evaluation for field points near boundaries will be recommended. In particular, we offer numerical results of the double divergence by the direct integral method and the finite difference method without requiring any body fitted volume grid.

The rest of the paper is organized as follows. In section II, the spectral collocation method used in this investigation is described and its application to problems with smooth boundaries is studied. We will demonstrate the exponential rate of convergence of the method and estimate Nodes per Wavelength required for a given order of the basis functions used. Computation of double divergence of the exact Green's function will also be discussed. In section III, we focus on the treatment of geometric corners of the boundary and study in detail the element refinement technique. In section IV, an example of applying the exact Green's function in a linear acoustic wave generation problem is presented in which the far-field sound obtained by an acoustic analogy equation is compared with that of the direct time-domain finite difference solution. Section V has the conclusions.

## II. Spectral Collocation Boundary Element Method

# A. Boundary Integral Equation for the Exact Green's Function

The boundary integral equation is formulated from a partial differential equation (PDE) for an exact Green's function,  $q(\mathbf{x}, \mathbf{y}, t, s)$ , which is defined as the solution to the convective wave equation<sup>5</sup>

$$\left(\frac{\partial}{\partial t} + \mathbf{U} \cdot \nabla\right)^2 g(\mathbf{x}, \mathbf{y}, t, s) - \nabla^2 g(\mathbf{x}, \mathbf{y}, t, s) = \delta(t - s)\delta(\mathbf{x} - \mathbf{y})$$
(1)

with boundary condition for its normal derivative

$$\frac{\partial g}{\partial n} = 0 \tag{2}$$

on all solid surfaces, where

$$\nabla \equiv \left(\frac{\partial}{\partial x_1}, \frac{\partial}{\partial x_2}, \frac{\partial}{\partial x_3}\right)$$

In equation (1),  $\mathbf{y}$  is a fixed source point or far-field point and  $\mathbf{x} = (x_1, x_2, x_3)$  is a field point where the solution is desired. Bold-faced variables indicate vectors or matrices. The uniform mean flow is assumed to be in the direction of  $x_1$  only, and is defined as  $\mathbf{U} = (M, 0, 0)$  where M is the Mach number. For this paper, only cylindrical bodies with constant cross-sections will be considered, making the resulting boundary integral equation (BIE) independent of a third variable,  $x_3$ . A BIE for  $g(\mathbf{x}, \mathbf{y}, t, s)$  in the frequency domain with reduced dimension, given by  $G_B(\overline{\mathbf{x}}, \overline{\mathbf{y}}, \overline{\omega})$ , is<sup>5</sup>

$$C_{s}G_{B}(\overline{\mathbf{z}}_{s}, \overline{\mathbf{y}}, \overline{\omega}) = G_{0}(\overline{\mathbf{y}}, \overline{\mathbf{z}}_{s}, \overline{\omega}) + \int_{C} i\omega U_{n}G_{0}(\overline{\mathbf{x}}_{s}, \overline{\mathbf{z}}_{s}, \overline{\omega})G_{B}(\overline{\mathbf{x}}_{s}, \overline{\mathbf{y}}, \overline{\omega})d\overline{\mathbf{x}}_{s}$$

$$- \int_{C} G_{1}(\overline{\mathbf{x}}_{s}, \overline{\mathbf{z}}_{s}, \overline{\omega})G_{B}(\overline{\mathbf{x}}_{s}, \overline{\mathbf{y}}, \overline{\omega})d\overline{\mathbf{x}}_{s} - \int_{C} U_{n}U_{t}G_{0}(\overline{\mathbf{x}}_{s}, \overline{\mathbf{z}}_{s}, \overline{\omega})\frac{\partial G_{B}(\overline{\mathbf{x}}_{s}, \overline{\mathbf{y}}, \overline{\omega})}{\partial \overline{x}_{s}}d\overline{\mathbf{x}}_{s}$$

$$(3)$$

where

$$G_0(\overline{\mathbf{y}}, \overline{\mathbf{z}}, \overline{\omega}) = \frac{i}{4\beta} e^{i\omega M(y_1 - z_1)/\beta^2} H_0^{(1)}(\overline{\omega r})$$
(4)

and

$$G_1(\overline{\mathbf{x}}, \overline{\mathbf{z}}, \overline{\omega}) = -\frac{i\overline{\omega}}{4\beta} e^{i\frac{\omega M(x_1 - z_1)}{\beta^2}} \frac{(\overline{\mathbf{x}} - \overline{\mathbf{z}}) \cdot \mathbf{n}}{\overline{r}} H_1^{(1)}(\overline{\omega r})$$
(5)

In equations (4) and (5),  $H_n^{(1)}(\overline{\omega r})$  is the nth-order Hankel function of the first kind and  $\beta = \sqrt{1 - M^2}$ . Throughout this paper, a barred variable denotes a two-dimensional vector. The terms  $U_n$  and  $U_t$  are the normal and tangential components of the mean flow and  $\mathbf{z}_s$  is a point on the boundary of the scatterer. The coefficient,  $C_s$ , in equation (3) is 1/2 on smooth boundary points. In order to solve the boundary integral equation for the exact Green's function, a spectral collocation boundary element method will be used.

## B. Formulation of the Boundary Element Method

After obtaining the boundary integral equation (3), the boundary is discretized into N "elements". The BIE is then required to be satisfied at fixed points, called collocation points, along each element. This leads to a system of linear equations, which are then written in matrix form in order to solve the BIE for the exact Green's function numerically.

Consider a boundary contour shown in Figure 1. Let the boundary of each element,  $\Gamma_i$ , be parameterized as

$$\overline{\mathbf{x}}_s = \mathbf{r}_j(t), t \in [0, 1] \tag{6}$$

where t is the local parameterization variable and  $\mathbf{r}_j(t)$  is the shape function for the jth element. The exact Green's function on each  $\Gamma_j$  is approximated by an expansion in a set of basis functions,  $\{\phi_n(t), n = 0, 1, 2, \dots, P\}$ , giving

$$G_B(\overline{\mathbf{x}}_s, \overline{\mathbf{y}}, \overline{\omega}) = G_B(\mathbf{r}_j(t), \overline{\mathbf{y}}, \overline{\omega}) = \sum_{n=0}^P u_j^{(n)} \phi_n(t)$$
 (7)

where  $u_j^{(n)}$  signifies the expansion coefficients and P represents the order of the expansion polynomials. Let the set of collocation points be defined as

$$\overline{\mathbf{z}}_s = \overline{\mathbf{z}}_i^{(\ell)}$$
 on element  $\Gamma_i$  where  $\overline{\mathbf{z}}_i^{(\ell)} = \mathbf{r}_i(t_\ell), \ell = 0, 1, ..., P$ 

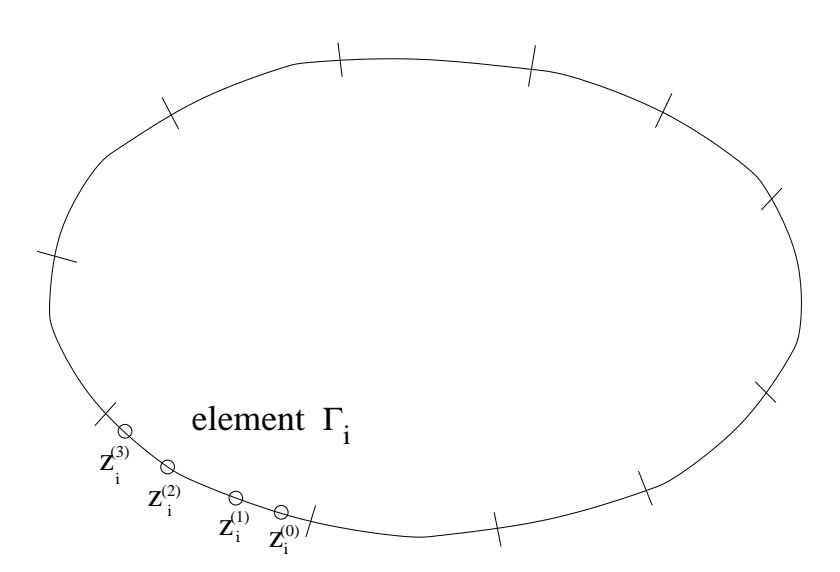


Figure 1. Schematic diagram showing boundary elements and collocation points

By substituting (7) into (3) and requiring (3) to be satisfied on the set of collocation points, the linear system of equations for the expansion coefficients,  $u_i^{(n)}$ , becomes<sup>5</sup>

$$\frac{1}{2} \sum_{n=0}^{P} u_i^{(n)} \phi_n(t_\ell) = G_0 \left( \overline{\mathbf{y}}, \overline{\mathbf{z}}_i^{(\ell)}, \overline{\omega} \right) + \sum_{j=1}^{N} \int_0^1 i\omega U_n G_0(\mathbf{r}_j(t), \overline{\mathbf{z}}_i^{(\ell)}, \overline{\omega}) \left[ \sum_{n=0}^{P} u_j^{(n)} \phi_n(t) \right] |\mathbf{r}_j'(t)| dt 
- \sum_{j=1}^{N} \int_0^1 G_1(\mathbf{r}_j(t), \overline{\mathbf{z}}_i^{(\ell)}, \overline{\omega}) \left[ \sum_{n=0}^{P} u_j^{(n)} \phi_n(t) \right] |\mathbf{r}_j'(t)| dt - \sum_{j=1}^{N} \int_0^1 U_n U_t G_0(\mathbf{r}_j(t), \overline{\mathbf{z}}_i^{(\ell)}, \overline{\omega}) \left[ \sum_{n=0}^{P} u_j^{(n)} \phi_n'(t) \right] dt \quad (8)$$

for  $\ell = 0, 1, ..., P$  and i = 1, ..., N. Chebyshev polynomials will be used as the basis functions and the collocation points will be the interior Gauss-Chebyshev points. The free-space Green's function (4) and its normal derivative (5) both have a logarithmic singularity when j = i, i.e., when the collocation point is on the element being integrated. However, these singularities can be removed as described in [4] and [5].

Once the expansion coefficients are computed, the exact Green's function can be found using equation (7). Finally, the second-order derivatives of the exact Green's function can be calculated and substituted into the acoustic analogy to determine the sound pressure.

## C. Numerical Solutions of a Circular Cylinder

### 1. Two-dimensional Solutions

Once the expansion coefficients,  $u_j^{(n)}$ , in the linear system are found, the value of the exact Green's function at any field point  $\overline{\mathbf{z}}$  located in the exterior domain is given by

$$G_{B}(\overline{\mathbf{z}}, \overline{\mathbf{y}}, \overline{\omega}) = G_{0}(\overline{\mathbf{y}}, \overline{\mathbf{z}}, \overline{\omega}) - \sum_{j=1}^{N} \int_{0}^{1} G_{1}(\mathbf{r}_{j}(t), \overline{\mathbf{z}}, \overline{\omega}) \left[ \sum_{n=0}^{P} u_{j}^{(n)} \phi_{n}(t) \right] |\mathbf{r}_{j}'(t)| dt$$

$$+ \sum_{j=1}^{N} \int_{0}^{1} i\omega U_{n} G_{0}(\mathbf{r}_{j}(t), \overline{\mathbf{z}}, \overline{\omega}) \left[ \sum_{n=0}^{P} u_{j}^{(n)} \phi_{n}(t) \right] |\mathbf{r}_{j}'(t)| dt - \sum_{j=1}^{N} \int_{0}^{1} U_{n} U_{t} G_{0}(\mathbf{r}_{j}(t), \overline{\mathbf{z}}, \overline{\omega}) \left[ \sum_{n=0}^{P} u_{j}^{(n)} \phi_{n}'(t) \right] dt$$
(9)

The double divergence of the exact Green's function is then calculated by taking spatial derivatives of equation (9). This results in<sup>5</sup>

$$\frac{\partial^{2}}{\partial z_{i}\partial z_{j}}G_{B}(\overline{\mathbf{z}},\overline{\mathbf{y}},\overline{\omega}) = \frac{\partial^{2}}{\partial z_{i}\partial z_{j}}G_{0}(\overline{\mathbf{y}},\overline{\mathbf{z}},\overline{\omega}) - \sum_{j=1}^{N} \int_{0}^{1} \frac{\partial^{2}}{\partial z_{i}\partial z_{j}}G_{1}(\mathbf{r}_{j}(t),\overline{\mathbf{z}},\overline{\omega}) \left[ \sum_{n=0}^{P} u_{j}^{(n)}\phi_{n}(t) \right] |\mathbf{r}_{j}'(t)| dt 
+ \sum_{j=1}^{N} \int_{0}^{1} i\omega U_{n} \frac{\partial^{2}}{\partial z_{i}\partial z_{j}}G_{0}(\mathbf{r}_{j}(t),\overline{\mathbf{z}},\overline{\omega}) \left[ \sum_{n=0}^{P} u_{j}^{(n)}\phi_{n}(t) \right] |\mathbf{r}_{j}'(t)| dt 
- \sum_{j=1}^{N} \int_{0}^{1} U_{n} U_{t} \frac{\partial^{2}}{\partial z_{i}\partial z_{j}}G_{0}(\mathbf{r}_{j}(t),\overline{\mathbf{z}},\overline{\omega}) \left[ \sum_{n=0}^{P} u_{j}^{(n)}\phi_{n}'(t) \right] dt \tag{10}$$

Equation (10) does not contain any logarithmic singularities because the field point,  $\overline{\mathbf{z}}$ , is not located on the boundary. Therefore, the integrals in equation (10) can theoretically be determined using Gaussian quadratures. A problem arises, however, when dealing with a field point that is very close to the boundary of the circular cross-section. The integral kernels in equation (10) are nearly singular on the element closest to the field point. To improve the accuracy of the double divergence, the interval of integration corresponding to the element closest to the field point is refined into subintervals that are grouped around the boundary point closest to the field point  $\overline{\mathbf{z}}$ . The integrals for each subinterval are then calculated using a 20-point Gaussian quadrature. The nearly singular integral kernels caused by the small distance between field point and element increase the error in the solution  $u_j^{(n)}$ . Consequently, the order P of the basis functions used when calculating the second derivatives of the Green's function must exceed the order of those used to calculate the Green's function to maintain the same accuracy.<sup>5</sup>

#### 2. Exponential Convergence for the Circular Cylinder

To demonstrate exponential convergence, consider a circular cylinder with constant cross-section of radius 0.5. Let the source point be located at  $\overline{\mathbf{y}}=(0,-20)$  and the frequency be  $\omega=4\pi$ . For this example, 16 boundary elements are used. In the case of the two-dimensional circular cylinder, the exact solution for M=0 is well known and therefore it is utilized in this section as the basis of comparison. For M=0.2, the numerical solution is compared with the values obtained using much higher order basis polynomials (P=15). The numerical errors at two sample field points for M=0 and M=0.2 are shown in Figures 2 and 3 respectively. The first field point (A) is located close to the boundary, at  $\overline{\mathbf{z}}=(0.51,0)$ , and the second point (B) is farther from the boundary, at  $\overline{\mathbf{z}}=(0.75,0)$ . Figures 2 and 3 show the spectral accuracy of the collocation method. For point (A), the errors corresponding to the second derivative of the Green's function are larger than those of the Green's function. This is a result of the nearly singular integral kernels discussed previously.

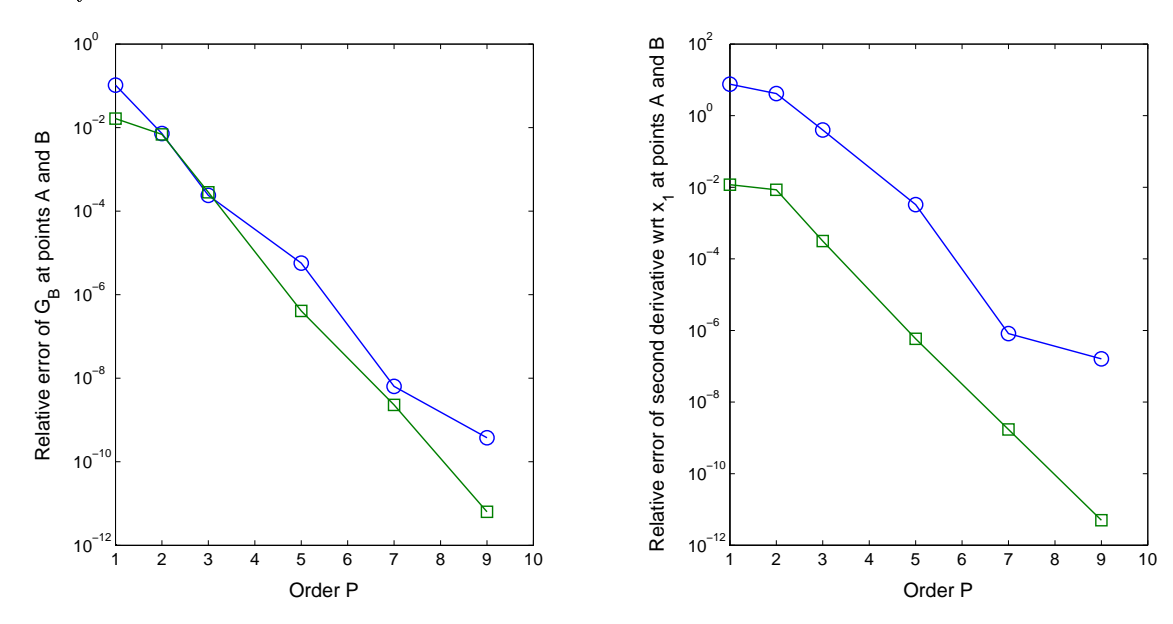


Figure 2. Relative error as a function of the order of basis polynomials for M=0. Circles:  $\overline{\mathbf{z}}=(0.51,0)$ ; Squares:  $\overline{\mathbf{z}}=(0.75,0)$ .

#### 3. Nodes per Wavelength Calculation

One advantage of using the spectral collocation BEM is that increasing the order of the basis functions increases the solution accuracy for a fixed number of nodal points. To demonstrate this property, a "nodes per wavelength" calculation will be performed. This is done by using the equation

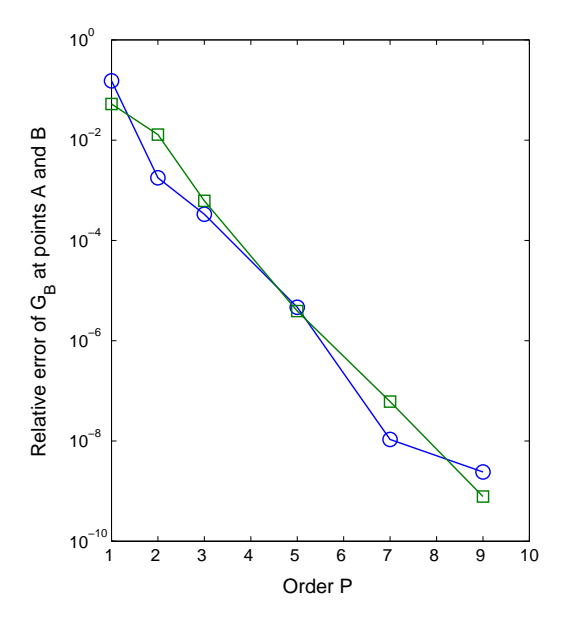
$$NPW = \frac{\widetilde{N}}{N_w} \tag{11}$$

In equation (11),  $\widetilde{N} = N(P+1)$  where N is the number of elements and P is the order of the basis functions.  $N_w$  is defined as the number of waves on arc length L and is given by

$$N_w = \frac{L}{\lambda}$$

where  $\lambda = \frac{2\pi}{\omega}$  for a given frequency  $\omega$ .

Consider again the circular cylinder with constant cross-section of radius 0.5, and choose twenty equally spaced field points for a given radius. Let the combined maximum allowable relative error be 0.005 when



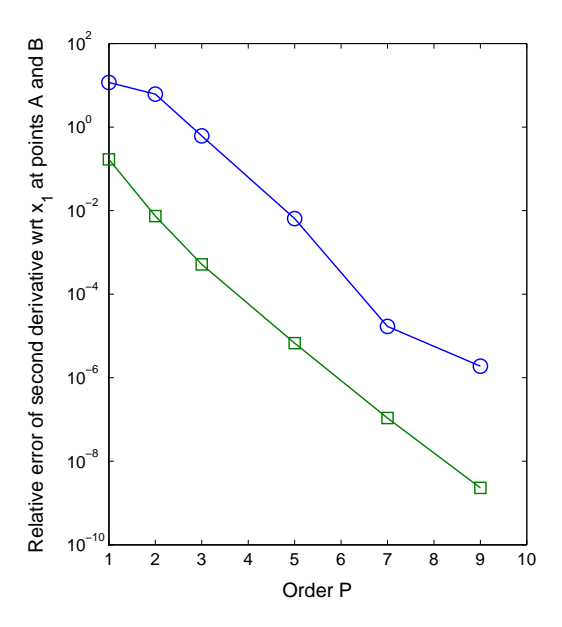


Figure 3. Relative error as a function of the order of basis polynomials for M=0.2. Circles:  $\overline{\mathbf{z}}=(0.51,0)$ ; Squares:  $\overline{\mathbf{z}}=(0.75,0)$ .

compared with the exact solution for M=0 and frequency  $40\pi$ . Tables 1 and 2 contain results for the Green's function and its second derivative with respect to  $x_1$  respectively. According to Tables 1 and 2, the computation time for field points at radius 0.51 is always greater for the same order than that for field points at radius 0.75. This is due to the computation time necessary for a refinement of the intervals of integration for a field point located close to the boundary. Also, in each case there is an optimal order in terms of computation time that is not necessarily the highest order. This is due to the number of quadrature points, 2(P+1), required to compute each integral in equation (8).

### 4. Finite Difference Approach

All spatial second derivative calculations of the Green's function thus far have been done using direct differentiation, as shown in equation (10). As previously discussed, for a field point close to the boundary, the integral kernels are nearly singular. Therefore, the solution errors are quite large, especially for smaller order basis function approximations.

An alternate method for calculating the double divergence is to use a finite difference method. For this paper, two finite difference stencils were applied to several field points, all located at a radius of 0.51 from the center of a circle of radius 0.5. The schemes used were a fourth-order central scheme given by

$$\frac{\partial^2 G_B}{\partial x_1^2} (x_1, x_2) = \left[ -G_B (x_1 + 2\Delta x, x_2) + 16G_B (x_1 + \Delta x, x_2) - 30G_B (x_1, x_2) \right] 
+ 16G_B (x_1 - \Delta x, x_2) - G_B (x_1 - 2\Delta x, x_2) / 12\Delta x^2$$
(12)

and a fourth-order forward scheme given by

$$\frac{\partial^2 G_B}{\partial x_1^2} (x_1, x_2) = \left[ 11 G_B (x_1, x_2) - 20 G_B (x_1 + \Delta x, x_2) + 6 G_B (x_1 + 2 \Delta x, x_2) \right] 
+ 4 G_B (x_1 + 3 \Delta x, x_2) - G_B (x_1 + 4 \Delta x, x_2) / 12 \Delta x^2$$
(13)

In the central scheme, the finite difference approximation was computed using  $\Delta x = 0.0005$ . In the forward scheme, two values for  $\Delta x$  were used; (a)  $\Delta x = 0.05$  and (b)  $\Delta x = 0.005$ . Basis functions of orders P = 2 and

Table 1. Nodes per wavelength and computation time required for a maximum relative error of 0.005 as the order of the basis polynomial P increases. The frequency is  $40\pi$  and the mean flow Mach number is M=0. Results for 20 field points at radius 0.51 for (a) Green's function and (b) its second derivative with respect to  $x_1$  are shown.

#### (a) Green's Function

Order	Number of	Nodes per	Computation Time
P	Nodes, $\widetilde{N}$	Wavelength, $NPW$	(seconds)
1	3800	60.4789	535.1094
2	855	13.6077	29.5313
3	432	6.8755	12.5156
5	360	5.7296	11.8281
7	312	4.9656	14.6406
9	300	4.7746	15.9375
11	276	4.3927	17.7813

## (b) Second derivative of Green's Function with respect to $x_1$

Order	Number of	Nodes per	Computation Time
P	Nodes, $\widetilde{N}$	Wavelength, $NPW$	(seconds)
1	4200	66.8451	689.6875
2	897	14.2762	32.2813
3	492	7.8304	15.4219
5	396	6.3025	15.4063
7	320	5.0930	13.7188
9	310	4.9338	15.9531
11	288	4.5837	18.1563

P=3 were used to calculate the Green's functions at the locations needed for equations (12) and (13). The scheme given by equation (12) produced similar values to the direct second derivative calculations. When equation (13) was used, both (a)  $\Delta x = 0.05$  and (b)  $\Delta x = 0.005$  gave improved results, however, none were significantly better. Hence, direct calculation is the preferred method for determining the double divergence of all field points, even those close to the boundary.

### III. Treatment of Geometric Discontinuities

## A. Nature of Corner Singularities

The spectral collocation boundary element method is very successful when applied to problems with smooth boundaries. However, when sharp angles such as corners are introduced into the boundary, the BEM alone will not result in exponential convergence because of these singular locations. The exact Green's function will not be analytic on corner elements and therefore, it cannot be adequately represented by Chebyshev polynomials. In fact, most standard methods for solving boundary value problems provide slow convergence and inaccurate solutions in the neighborhood of a corner singularity.<sup>8</sup>

For the case of a two-dimensional exterior domain governed by a Helmoltz equation with homogeneous Neumann boundary conditions on the corner edges, the asymptotic expansion of a singular solution at a

Table 2. Nodes per wavelength and computation time required for a maximum relative error of 0.005 as the order of the basis polynomial P increases. The frequency is  $40\pi$  and the mean flow Mach number is M=0. Results for 20 field points at radius 0.75 for (a) Green's function and (b) its second derivative with respect to  $x_1$  are shown.

### (a) Green's Function

Order	Number of	Nodes per	Computation Time
P	Nodes, $\widetilde{N}$	Wavelength, $NPW$	(seconds)
1	3140	49.9747	314.8594
2	774	12.3186	17.3594
3	420	6.6845	6.7031
5	354	5.6341	7.3281
7	312	4.9656	7.8906
9	300	4.7746	9.3281
11	276	4.3927	9.9219

## (b) Second derivative of Green's Function with respect to $x_1$

Order	Number of	Nodes per	Computation Time
P	Nodes, $\widetilde{N}$	Wavelength, $NPW$	(seconds)
1	4200	66.8451	665.8281
2	894	14.2285	22.7344
3	484	7.7031	8.5938
5	360	5.7296	7.2813
7	320	5.0929	7.9531
9	300	4.775	9.0156
11	288	4.5837	10.2656

corner is

$$g(r,\theta) = \sum_{p=0}^{\infty} a_p g_p(r,\theta) = \sum_{p=0}^{\infty} a_p J_{p\alpha} \left( kr \rho(\theta) \right) \cos(\eta)$$
(14)

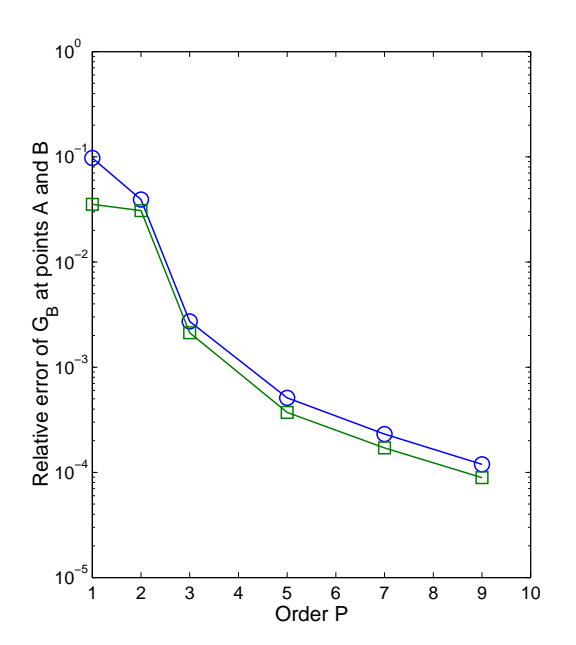
where  $\alpha = \frac{\pi}{\xi}$  and  $\eta$  is a function of  $\theta$ .<sup>8</sup> In equation (14),  $\xi$  is defined as the exterior angle of the corner. For  $\text{Re}(p\alpha) \geq 0$ , the Bessel function of the first kind in equation (14) can be approximated by its asymptotic expansion for  $z \to 0$  as

$$J_{p\alpha}(z) \sim \frac{1}{\Gamma(p\alpha+1)} \left(\frac{z}{2}\right)^{p\alpha} = C_p z^{p\alpha}$$
 (15)

where  $z = kr\rho(\theta)$ . Since  $\alpha$  is not always an integer, the singular solution given in equation (14) could contain irrational expressions of r. The convergence of a spectral series for a function is controlled by the "singularities" of that function.<sup>1</sup> The term "singularities" includes poles, fractional powers, branch points, and discontinuities of the function or its derivatives.

## B. Results of Spectral Collocation BEM on a Square Boundary

To demonstrate the slow convergence of the collocation method when applied to non-smooth boundaries, consider a square centered at the origin with corners located at (0.5, 0.5), (0.5, -0.5), (-0.5, -0.5) and (-0.5, 0.5). The two sample field points analyzed will again be (A)  $\overline{\mathbf{z}} = (0.51, 0)$  and (B)  $\overline{\mathbf{z}} = (0.75, 0)$ . The source point location is  $\overline{\mathbf{y}} = (0, -20)$ , the frequency is  $\omega = 4\pi$  and the number of elements is N = 16. Table



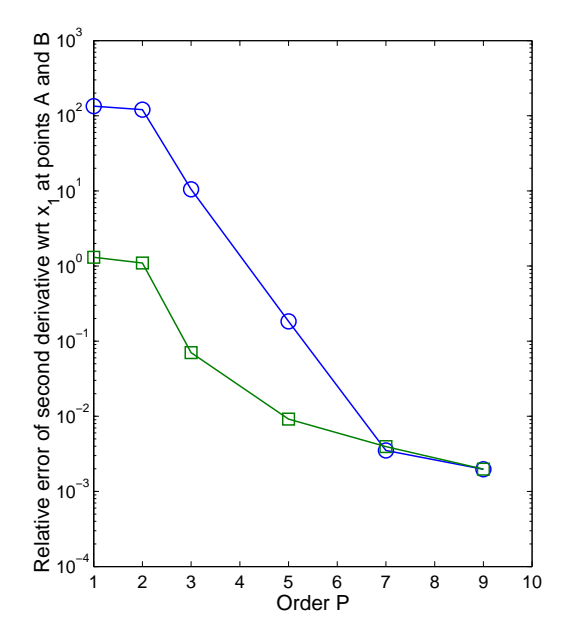


Figure 4. Relative error as a function of the order of basis polynomials for square boundary with M=0. Circles:  $\overline{\mathbf{z}}=(0.51,0)$ ; Squares:  $\overline{\mathbf{z}}=(0.75,0)$ .

3 shows the relative errors for the Green's function,  $G_B$ , and its second derivative,  $\frac{\partial^2 G_B}{\partial x_1^2}$  when compared with a high order (P=15) solution. The data for Table 3 are also plotted in Figure 4. Table 3 and Figure

Table 3. Relative errors of exact Green's function and its second derivative with respect to  $x_1$  as the order P increases. The number of elements on the square's boundary is N=16 and the frequency is  $4\pi$ . The mean flow Mach number is M=0.

Order	Point A	$\overline{\mathbf{z}} = (0.51, 0)$	Point B	$\overline{\mathbf{z}} = (0.75, 0)$
P	$G_B$	$\frac{\partial^2 G_B}{\partial x_1^2}$	$G_B$	$\frac{\partial^2 G_B}{\partial x_1^2}$
1	0.0973225	133.980	0.0353173	1.30873
2	0.0392499	120.398	0.0308039	1.09711
3	0.00272320	10.4763	0.00212314	0.0704248
5	0.000510972	0.183188	0.000371261	0.00917916
7	0.000231130	0.00350694	0.000170683	0.00394068
9	0.000119278	0.00197095	0.0000890705	0.00197641

4 show that a non-exponential rate of decay occurs as the order of the basis polynomials increases. In the attempt to improve these results, an exponential grading mesh refinement will be performed on all corner elements.

## C. Exponential Grading Mesh Refinement

#### 1. Results for a Fixed Refinement Ratio

Many approaches have been used to reduce the discretization errors associated with geometric singularities. A common approach involves the use of singular elements that require the orders of the singularities to be included at the corresponding singular nodes. Ong and Lim<sup>9</sup> successfully applied this method to three-dimensional potential problems. Another technique used to overcome corner singularities incorporates

complex mapping into the BEM. This method has been explored by Wang and Tsay<sup>11</sup> as well as by Boyd.<sup>2</sup> A third technique developed in recent years by Igarashi and Honma<sup>6</sup> and Marin et al.<sup>8</sup> involves subtracting the singularities from the original potential function. These singularities behave like  $r^{(p\alpha)}$  for p = 0, 1, 2, ..., as shown in equation (15). If  $\alpha$  is not an integer, many terms may have to be subtracted to successfully utilize this approach, which can make finding a solution more tedious.

One of the most successful techniques is the h-version mesh refinement method. In this approach, the order of the basis functions is kept constant, while the number of elements in the neighborhood of the singularity is increased. The resulting singular elements make up a small percentage of the total number of elements, thereby decreasing the errors caused by the singularities. In general, a power convergence rate is obtained when the h-version is applied in solving a Helmholtz equation problem. If h is the element size, the error decreases as  $h^{(P+1)}$  for  $h \to 0$ , where P is the order of the basis functions. One advantage of mesh refinement methods is that no prior knowledge of the singularity behavior is required. Only the locations of the singularities must be known. This property, along with the convergence rate, makes the h-version mesh refinement method a more robust method for dealing with changes in geometry.

For this paper, an exponential grading mesh refinement is applied to the square described in the previous section. The refinement is given by  $\rho^{N_g}$ , where  $\rho$  is the refinement ratio and  $N_g$  is the level of refinement. The value of  $\rho$  is in (0,1] where  $\rho=1$  would produce the original number of elements. In the following example, each element containing a corner point is refined using the same refinement ratio and level of refinement.

For the 16-element square, let  $\rho=0.35$  and  $N_g=P+2$ , where P is the order of the basis functions. The frequency is  $\omega=4\pi$  and the source point is located at  $\overline{\mathbf{y}}=(0,-20)$ . For comparison purposes, we will again look at field points (A)  $\overline{\mathbf{z}}=(0.51,0)$  and (B)  $\overline{\mathbf{z}}=(0.75,0)$ . Table 4 shows the relative errors for the Green's function,  $G_B$ , and its second derivative,  $\frac{\partial^2 G_B}{\partial x_1^2}$  when compared with an order P=15 solution for M=0. The results are also plotted in Figure 5.

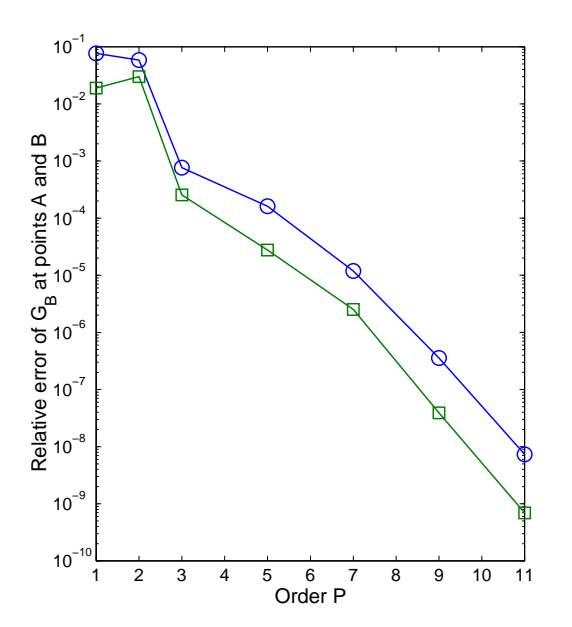
Table 4. Relative errors of exact Green's function and its second derivative with respect to  $x_1$  as the order P increases. The frequency is  $4\pi$ ,  $\rho = 0.35$  and  $N_q = P + 2$ . The mean flow Mach number is M = 0.

Order	Point A	$\overline{\mathbf{z}} = (0.51, 0)$	Point B	$\overline{\mathbf{z}} = (0.75, 0)$
P	$G_B$	$\frac{\partial^2 G_B}{\partial x_1^2}$	$G_B$	$\frac{\partial^2 G_B}{\partial x_1^2}$
1	0.0763597	132.533	0.0188810	1.23859
2	0.0584410	139.445	0.0300076	1.09480
3	0.000764934	21.4354	0.000255573	0.0510741
5	0.000161642	2.35153	0.0000276648	0.00172533
7	0.0000118897	0.0801876	2.51755E - 06	0.000184259
9	3.57358E - 07	0.0000460827	3.91149E - 08	3.45152E - 06
11	7.31339E - 09	0.0000895887	6.93006E - 10	2.67518E - 08

## 2. Effects of Changing the Refinement Ratio

All calculations made for the previous section were done for a fixed refinement ratio,  $\rho$ , and level of refinement,  $N_g$ . To determine the best mesh refinement strategy, many values of  $\rho$  and  $N_g$  have been tested. Of course, a value of  $\rho$  that is too close to one (1) would not be ideal because there would not be enough of a refinement. Also, any increase in  $N_g$  causes an increase in the number of elements, resulting in higher computation time. Therefore, lower levels of refinement are preferred.

Consider the square boundary discussed previously. Table 5 illustrates the effects of changing  $\rho$  and  $N_g$ . The order of the basis functions was kept constant (P=7) for this comparison. According to Table 5, changing the refinement ratio has a greater effect on the relative errors than increasing the level of refinement.



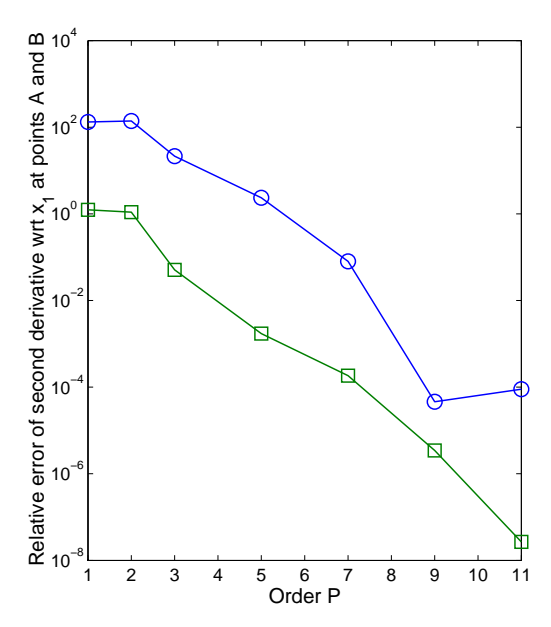


Figure 5. Relative error as a function of the order of basis polynomials for square boundary with M=0. Mesh refinement with  $\rho=0.35$  and  $N_q=P+2$ . Circles:  $\overline{\mathbf{z}}=(0.51,0)$ ; Squares:  $\overline{\mathbf{z}}=(0.75,0)$ .

Another strategy is to keep the last refinement on each corner element, given by  $\rho^{N_g}$ , constant. Two values for the refinement, (a)  $\rho^{N_g} \approx 0.05$  and (b)  $\rho^{N_g} \approx 0.008$ , were studied, and the results are given in Figures 6 and 7. In both cases, the field point is located at  $\overline{\mathbf{z}} = (0.75, 0)$ . Figure 6 shows that for all values of  $\rho$  and  $N_g$ , the results for both  $G_B$  and  $\frac{\partial^2 G_B}{\partial x_1^2}$  are improved over the results of no mesh refinement. However, according to Figure 7,  $\rho = 0.09$  with  $N_g = 2$  gives the largest errors for both the Green's function and its second derivative, showing that there is a minimum as well as a maximum value for the refinement ratio.

# IV. An example

There are very few exact solutions that can be used for validating an acoustic analogy calculation. Comparison with experimental results has been an important means of evaluating noise predicting strategies. In this section, we formulate an acoustic analogy example for the linear Euler equation and compare the predicted sound field obtained by using the exact Green's function discussed above with that of a direct time-domain finite difference solution.

Consider the continuity and momentum equations in conservation form as

Table 5. Relative errors of the Green's function using exponential grading mesh refinement for the square boundary. The frequency is  $4\pi$ , the mean flow Mach number is M=0 and the source point is located at  $\overline{y}=(0,-20)$ .

Level of Refinement	$\rho = 0.85$	$\rho = 0.5$	$\rho = 0.35$
$N_g = 2$	6.30136E - 05	2.01483E - 05	1.07959E - 05
$N_g = 3$	5.24537E - 05	1.14010E - 05	5.53004E - 06
$N_g = 4$	4.39122E - 05	7.59983E - 06	3.73803E - 06
$N_g = 5$	3.70199E - 05	5.85945E - 06	
$N_g = 6$	3.14598E - 05		
$N_g = 7$	2.69720E - 05		

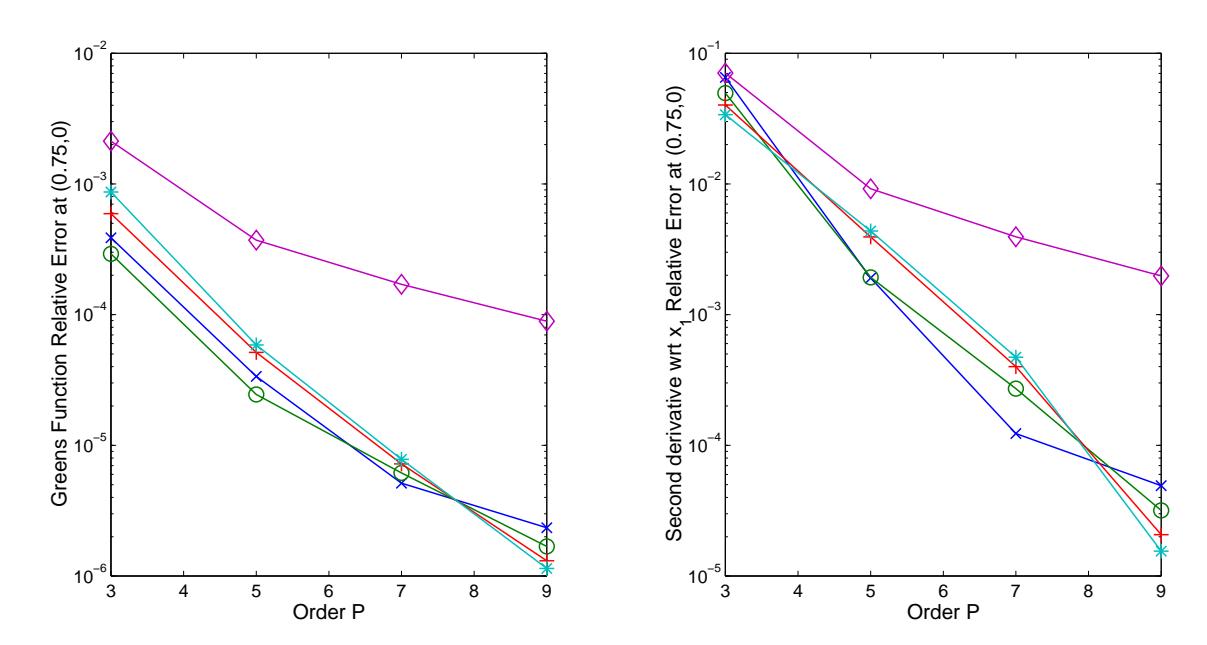


Figure 6. Relative error as a function of the order of basis polynomials for square boundary with M=0. Mesh refinement with  $\rho^{Ng}\approx 0.05$ . Cross:  $\rho=0.223$  and  $N_g=2$ ; Circle:  $\rho=0.37$  and  $N_g=3$ ; Plus:  $\rho=0.55$  and  $N_g=5$ ; Star:  $\rho=0.65$  and  $N_g=7$ ; Diamond: No mesh refinement.

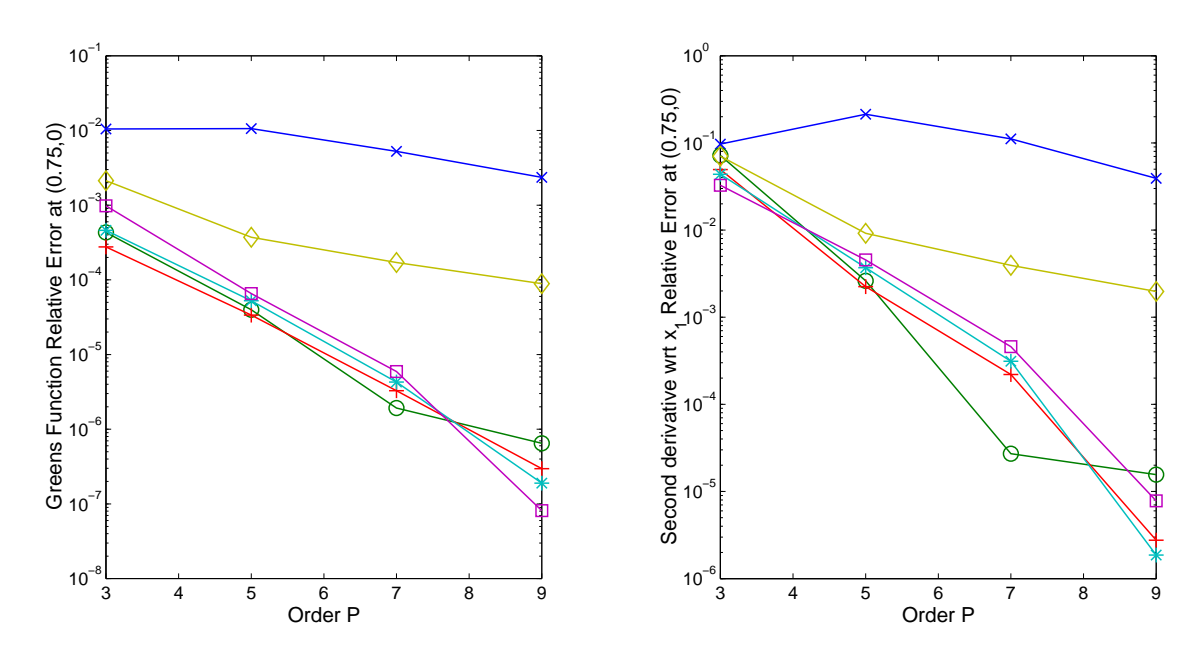


Figure 7. Relative error as a function of the order of basis polynomials for square boundary with M=0. Mesh refinement with  $\rho^{N_g}\approx 0.008$ . Cross:  $\rho=0.09$  and  $N_g=2$ ; Circle:  $\rho=0.2$  and  $N_g=3$ ; Plus:  $\rho=0.38$  and  $N_g=5$ ; Star:  $\rho=0.5$  and  $N_g=7$ ; Square:  $\rho=0.69$  and  $N_g=13$ ; Diamond: No mesh refinement.

$$\frac{\partial \rho}{\partial t} + \frac{\partial \rho u_1}{\partial x_1} + \frac{\partial \rho u_2}{\partial x_2} = 0 \tag{16}$$

$$\frac{\partial \rho u_1}{\partial t} + \frac{\partial \rho u_1 u_1}{\partial x_1} + \frac{\partial \rho u_1 u_2}{\partial x_2} + \frac{\partial p}{\partial x_1} = 0 \tag{17}$$

$$\frac{\partial \rho u_2}{\partial t} + \frac{\partial \rho u_1 u_2}{\partial x_1} + \frac{\partial \rho u_2 u_2}{\partial x_2} + \frac{\partial p}{\partial x_2} = 0 \tag{18}$$

where effects of viscosity are ignored. To form the acoustic analogy equation with the convective effect of a far-field constant mean flow included, we re-write the above as

$$\frac{\partial \rho}{\partial t} + u_{\infty} \frac{\partial \rho}{\partial x_1} + \frac{\partial \rho(u_1 - u_{\infty})}{\partial x_1} + \frac{\partial \rho u_2}{\partial x_2} = 0$$
(19)

$$\frac{\partial \rho u_1}{\partial t} + u_{\infty} \frac{\partial \rho u_1}{\partial x_1} + \frac{\partial \rho (u_1 - u_{\infty}) u_1}{\partial x_1} + \frac{\partial \rho u_1 u_2}{\partial x_2} + \frac{\partial p}{\partial x_1} = 0$$
 (20)

$$\frac{\partial \rho u_2}{\partial t} + u_{\infty} \frac{\partial \rho u_2}{\partial x_1} + \frac{\partial \rho (u_1 - u_{\infty}) u_2}{\partial x_1} + \frac{\partial \rho u_2 u_2}{\partial x_2} + \frac{\partial p}{\partial x_2} = 0$$
 (21)

where  $u_{\infty}$  is the constant mean velocity in the  $x_1$ - direction. By taking the operation  $\left(\frac{\partial}{\partial t} + u_{\infty} \frac{\partial}{\partial x_1}\right)$  (19) –  $\frac{\partial}{\partial x_1}$  (20) –  $\frac{\partial}{\partial x_2}$  (21), it is straight-forward to obtain the following acoustic analogy equation:

$$\left(\frac{\partial}{\partial t} + u_{\infty} \frac{\partial}{\partial x_{1}}\right)^{2} \rho - a_{\infty}^{2} \left(\frac{\partial^{2} \rho}{\partial x_{1}^{2}} + \frac{\partial^{2} \rho}{\partial x_{2}^{2}}\right) = \frac{\partial^{2} T_{11}}{\partial x_{1}^{2}} + 2 \frac{\partial^{2} T_{12}}{\partial x_{1} \partial x_{2}} + \frac{\partial^{2} T_{22}}{\partial x_{2}^{2}}$$
(22)

where

$$T_{11} = \rho(u_1 - u_{\infty})(u_1 - u_{\infty}) + p - a_{\infty}^2 \rho$$

$$T_{12} = \rho(u_1 - u_{\infty})u_2$$

$$T_{22} = \rho u_2 u_2 + p - a_{\infty}^2 \rho$$

and  $a_{\infty}$  is the speed of sound. We will consider a perturbed flow

$$\rho = \bar{\rho} + \rho', \ u_1 = \bar{u}_1 + u_1', \ u_2 = \bar{u}_2 + u_2'$$

where the mean velocity field is given by the potential flow over a circular cylinder as

$$\bar{u}_1 = u_{\infty} (1 - \frac{r_0^2}{r^2} \cos(2\theta)), \quad \bar{u}_2 = -u_{\infty} \frac{r_0^2}{r^2} \sin(2\theta)$$
 (23)

The perturbed flow is initialized with a vortex far away from the cylinder where the mean flow is close to the uniform velocity  $u_{\infty}$ , i.e., at t=0, we have

$$\rho' = 0, \ u_1' = (x_2 - 0.85)e^{-\ln(2)\left(\frac{(x_1 + 2.5)^2 + (x_2 - 0.85)}{0.04}\right)}, \ u_2' = -(x_1 + 2.5)e^{-\ln(2)\left(\frac{(x_1 + 2.5)^2 + (x_2 - 0.85)}{0.04}\right)}$$
(24)

The perturbed flow is solved first by linearized equations of (16)-(18) using a finite difference scheme. The linearized equations in primitive variables are

$$\frac{\partial \rho'}{\partial t} + \bar{\rho} \frac{\partial u_1'}{\partial x_1} + \bar{\rho} \frac{\partial u_2'}{\partial x_2} + \frac{\partial \bar{\rho}}{\partial x_1} u_1' + \frac{\partial \bar{\rho}}{\partial x_2} u_2' + \bar{u}_1 \frac{\partial \rho'}{\partial x_1} + \bar{u}_2 \frac{\partial \rho'}{\partial x_2} + [\frac{\partial \bar{u}_1}{\partial x_1} + \frac{\partial \bar{u}_2}{\partial x_2}] \rho' = 0$$
 (25)

$$\frac{\partial u_1'}{\partial t} + \bar{u}_1 \frac{\partial u_1'}{\partial x_1} + \bar{u}_2 \frac{\partial u_1'}{\partial x_2} + \frac{\partial \bar{u}_1}{\partial x_1} u_1' + \frac{\partial \bar{u}_1}{\partial x_2} u_1' + \frac{1}{\bar{\rho}} [\bar{u}_1 \frac{\partial \bar{u}_1}{\partial x_1} + \bar{u}_2 \frac{\partial \bar{u}_1}{\partial x_2}] \rho' + \frac{a_{\infty}^2}{\bar{\rho}} \frac{\partial \rho'}{\partial x_1} = 0$$
 (26)

$$\frac{\partial u_2'}{\partial t} + \bar{u}_1 \frac{\partial u_2'}{\partial x_1} + \bar{u}_2 \frac{\partial u_2'}{\partial x_2} + \frac{\partial \bar{u}_2}{\partial x_1} u_1' + \frac{\partial \bar{u}_2}{\partial x_2} u_2' + \frac{1}{\bar{\rho}} [\bar{u}_1 \frac{\partial \bar{u}_2}{\partial x_1} + \bar{u}_2 \frac{\partial \bar{u}_2}{\partial x_2}] \rho' + \frac{a_\infty^2}{\bar{\rho}} \frac{\partial \rho'}{\partial x_2} = 0$$
 (27)

in which we have assumed, for simplicity,  $p' = a_{\infty}^2 \rho'$ .

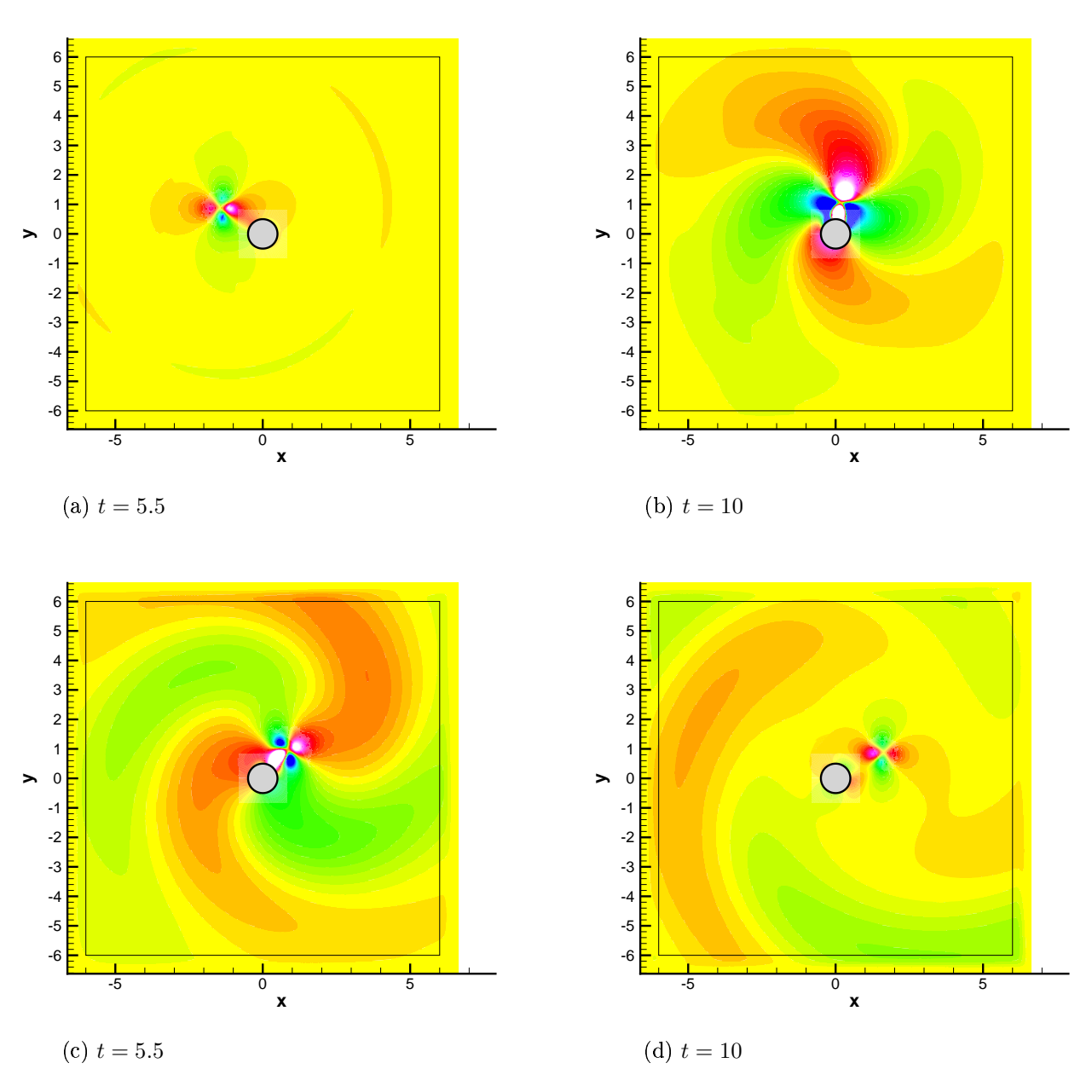


Figure 8. Instantaneous density contours.

Figure 8 shows the time-domain finite difference solution by (25)-(27). Initially, the vortex will be in a translational motion without significant sound emission. As it passes the cylinder, due to the non-uniform mean flow around the cylinder, acoustic waves are generated as shown in Figure 8 (a)-(d).

The far-field acoustic wave can also be obtained through an acoustic analogy equation. From (25)-(27), it can be easily verified that the density perturbation will satisfy the following linearized acoustic analogy equation

$$\left(\frac{\partial}{\partial t} + u_{\infty} \frac{\partial}{\partial x_1}\right)^2 \rho' - a_{\infty}^2 \left(\frac{\partial^2 \rho'}{\partial x_1^2} + \frac{\partial^2 \rho'}{\partial x_2^2}\right) = \frac{\partial^2 T'_{11}}{\partial x_1^2} + 2\frac{\partial^2 T'_{12}}{\partial x_1 \partial x_2} + \frac{\partial T'_{22}}{\partial x_2^2} \tag{28}$$

where  $T'_{11}$ ,  $T'_{12}$  and  $T'_{22}$  are the linearized stress tensors.

$$T'_{11} = 2\bar{\rho}(\bar{u}_1 - u_{\infty})u'_1 + (\bar{u}_1 - u_{\infty})(\bar{u}_1 - u_{\infty})\rho'$$

$$T'_{12} = \bar{\rho}(\bar{u}_1 - u_{\infty})u'_2 + \bar{\rho}\bar{u}_2u'_1 + (\bar{u}_1 - u_{\infty})\bar{u}_2\rho'$$

$$T_{22}' = 2\bar{\rho}\bar{u}_2u_2' + \bar{u}_2\bar{u}_2\rho'$$

To find the far-field sound by the acoustic analogy equation (28), we use its frequency-domain solution

$$\rho'(\mathbf{y},\omega) = \int_{V} T'_{ij}(\mathbf{x},\omega) \frac{\partial^{2} G_{B}(\mathbf{x},\mathbf{y},\omega)}{\partial x_{i} \partial x_{j}} dV$$
(29)

where  $G_B(\mathbf{x}, \mathbf{y}, \omega)$  is the exact Green's function discussed in previous sections using  $\mathbf{y}$  as the source (receiving) point with U = (-0.2, 0, 0). The frequency-domain stress tensor  $T'_{ij}(\mathbf{x}, \omega)$  is obtained by the Fast Fourier Transform (FFT) of the time-domain simulation. The volume integral of (29) is carried out in a finite region surrounding the cylinder, namely, 0.5 < r < 1.5, where  $T'_{ij}(\mathbf{x}, \omega)$  make the most significant contribution, as shown in Figure 9.

Figure 10 shows the density perturbation,  $\rho'(\mathbf{y}, \omega)$ , versus frequency for far-field points located at (A)  $\mathbf{y} = (-6, 0)$  and (B)  $\mathbf{y} = (0, -6)$  along with experimental results at both points. In general, the numerical results for point (A) are consistent with experimental data. However, at point (B), the numerical results are not as accurate. Future work will be done to try to reduce the errors at point (B) by enlarging the radius of integration and/or increasing the number of field points.

## V. Conclusions

The spectral collocation boundary element method proposed in [5] has been applied to both smooth and non-smooth boundaries. For smooth boundaries, exponential convergence has been demonstrated. A Nodes per Wavelength calculation was made to illustrate the benefits of using high-order basis functions. A finite difference approach for computing the double divergence has been introduced and compared to the direct differentiation approach, with direct calculation being the preferred method for all field points. To treat the geometric singularities of non-smooth boundaries, an exponential grading mesh refinement method was applied to a square boundary. Different mesh refinement strategies were compared and the effects of changing the refinement ratio were reported. It has been shown that proper mesh refinement yields exponential convergence for the square boundary. Finally, an example was done to compare the far-field sound density calculated using the acoustic analogy to direct numerical simulation results at two far-field points.

## Acknowledgement

This work is supported by a grant from the NASA Langley Research Center, NAG1-03037. The technical monitor is Dr. Mehdi R. Khorrami.

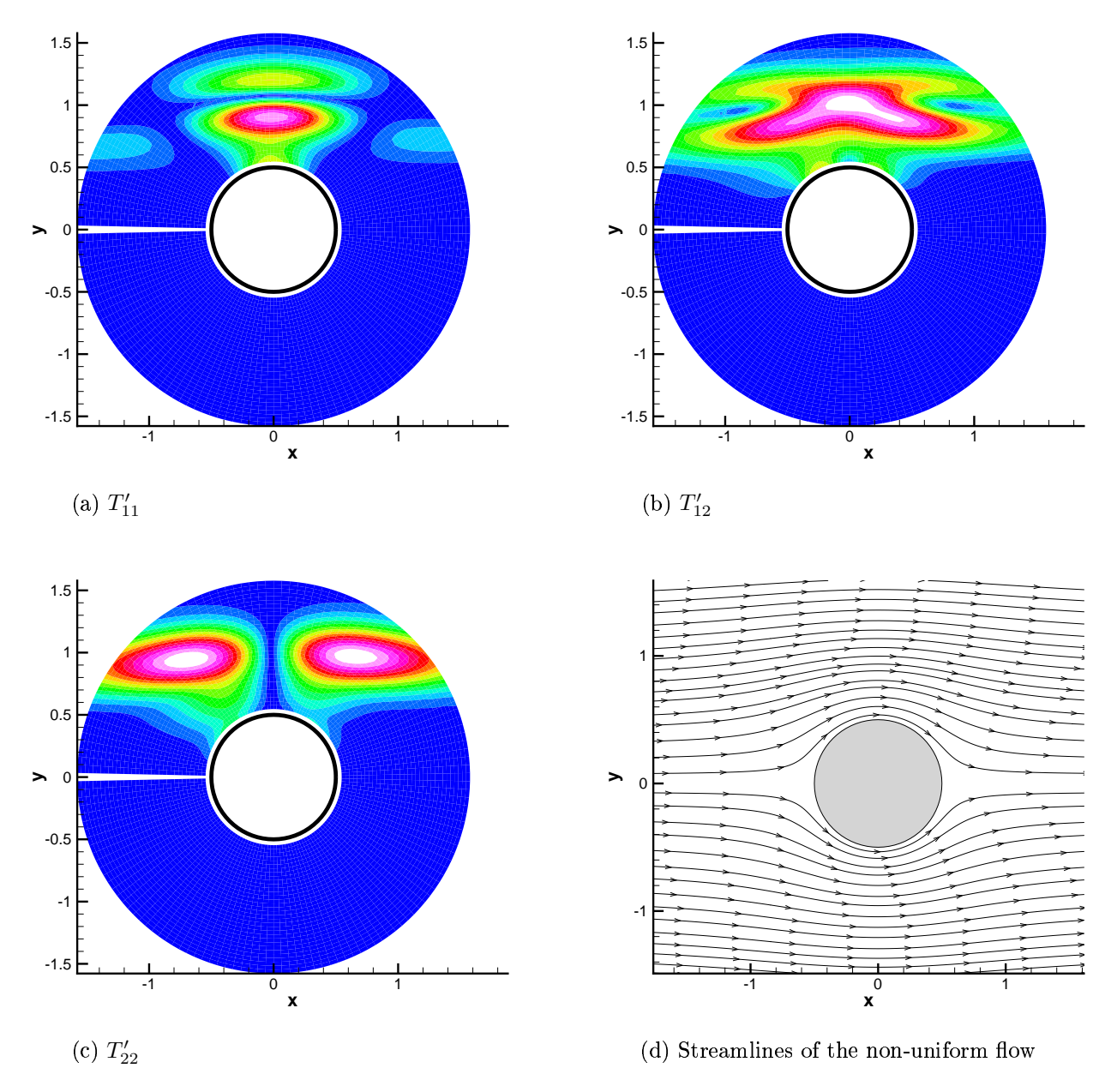
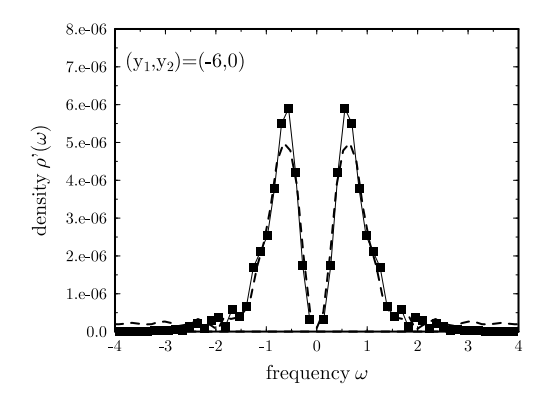


Figure 9. Contours of the stress tensor  $T_{ij}'$  at frequency  $\omega=0.98.$ 



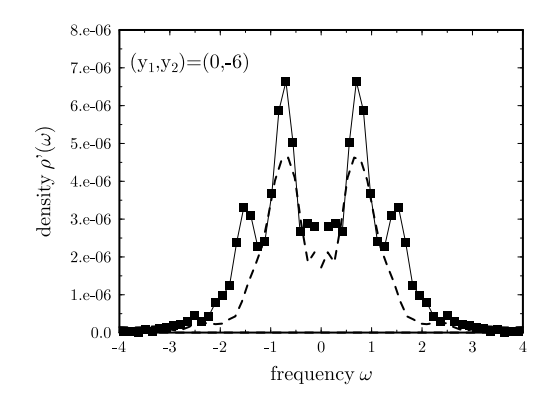


Figure 10. Density,  $\rho'(\omega)$ , as a function of frequency,  $\omega$ , at far-field points (A) y = (-6,0) and (B) y = (0,-6). Squares: acoustic analogy results; dotted line: direct numerical simulation results.

# References

- <sup>1</sup>J. P. Boyd, Chebyshev and fourier spectral methods. 2nd ed., Dover, 2000.
- <sup>2</sup>J. P. Boyd, "A Chebyshev/rational Chebyshev spectral method for the Helmholtz equation in a sector on the surface of a sphere: defeating corner singularities", Journal of Computational Physics, Vol. 206, No. 1, 302-310, 2005.
- <sup>3</sup>Y. P. Guo, "Airframe Noise Prediction by Acoustic Analogy", NASA Report NAS1-00086, 2004.
- <sup>4</sup>F. Q. Hu, "A spectral boundary integral equation method for the 2D Helmholtz equation", Journal of Computational Physics, Vol. 120, 340-347, 1995.
- <sup>5</sup>F. Q. Hu, Y. P. Guo and A. D. Jones, "On the computation and application of exact Green's function in acoustic analogy", AIAA paper 2005-2986.
- <sup>6</sup>H. Igarashi and T. Honma, "A boundary element method for potential fields with corner singularities", Appl. Math. Modelling, Vol. 20, 847-852,1996.
- <sup>7</sup>P. Juhl, "A note on the convergence of the direct collocation boundary element method", Journal of Sound and Vibration, Vol. 212, No. 4, 703-719, 1998.
- <sup>8</sup>L. Marin, D. Lesnic and V. Mantic, "Treatment of singularities in Helmholtz-type equations using the boundary element method", Journal of Sound and Vibration, Vol. 278, No. 1-2, 39-62, 2004.
- <sup>9</sup>E. T. Ong and K. M. Lim, "Three-dimensional singular boundary elements for corner and edge singularities in potential problems", Engrg. Anal. Bound. Elem., Vol. 29, 175-189, 2005.
- <sup>10</sup>E. P. Stephan, "The h-p boundary element method for solving 2- and 3-dimensional problems", Comput. Methods Appl. Mech. Engrg., Vol. 133, 183-208, 1996.
- <sup>11</sup>J. Wang and T. Tsay, "Analytical evaluation and application of the singularities in boundary element method", Engrg. Anal. Bound. Elem., Vol.29, 241-256, 2005.